INTERNATIONAL JOURNAL OF HYDROGEN ENERGY 45 (2020) 3035–3045

Available online at www.sciencedirect.com

ScienceDirect

journal homepage: www.elsevier.com/locate/he

Remarkable improvement in hydrogen storage capacities of two-dimensional carbon nitride (g-C_3N_4) nanosheets under selected transition metal doping

Puspamitra Panigrahi [a,**], *Ashok Kumar* [a], *Amir Karton* [b], *Rajeev Ahuja* [c,d], *Tanveer Hussain* [b,*]

[a] *Centre for Clean Energy and Nano Convergence, Hindustan Institute of Technology and Science, Chennai, 603103, Tamil Nadu, India*

[b] *School of Molecular Sciences, The University of Western Australia, Perth, WA, 6009, Australia*

[c] *Condensed Matter Theory Group, Department of Physics and Astronomy, Box 516, Uppsala University, S-75120, Uppsala, Sweden*

[d] *Applied Materials Physics, Department of Materials and Engineering, Royal Institute of Technology (KTH), S-100 44, Stockholm, Sweden*

HIGHLIGHTS

- Graphite carbon nitride (g-C_3N_4) sheet has been investigated as H_2 storage materials.
- Selected transition metals (TMs) and their dimers were used for the first time to decorate the g-C_3N_4 sheet.
- The stability of these TMs decorated g-C_3N_4 sheets have been confirmed with *ab-initio* molecular dynamics simulations.
- Dimers doped g-C_3N_4 sheet are found to be more promising for H_2 storage.
- Binding energy per H_2 molecule falls in the range of 0.3–0.7 eV/H_2, which is ideal for practical applications.

ARTICLE INFO

Article history:
Received 21 May 2019
Received in revised form
1 November 2019
Accepted 25 November 2019
Available online 19 December 2019

Keywords:
DFT
Monolayers
Adsorption
Metal dopants
Storage capacity

ABSTRACT

We have performed DFT simulations to quest for an optimal material for onboard hydrogen (H_2) storage applications. Using first-principles calculations, we established that the selected transition metals (M: Sc, Ti, Ni, V) decorated two-dimensional (2D) g-C_3N_4 sheets as optimal materials with reversible and significantly high H_2 gravimetric densities. By effectively avoiding metal-metal (M-M) clustering effect in case of mono doping, up to four molecules of H_2 per dopant could be adsorbed with an average binding energy of around 0.30–0.6 eV/H_2, which is ideal for practical applications. Decorating the g-C_3N_4 sheet with (M-M) dimers, the systems are found to be even more efficient for H_2 binding than single dopant decoration. The stability of these M decorated g-C_3N_4 sheets have been confirmed with *ab-initio* molecular dynamics simulations. We have further calculated the H_2 desorption temperatures of metal decorated g-C_3N_4 sheets, which confirms the practical application of these metal decorated sheets at ambient working conditions.

* *Corresponding author.*
** *Corresponding author.*
E-mail addresses: puspamitrap@hindustanuniv.ac.in (P. Panigrahi), tanveer.hussain@physics.uu.se (T. Hussain).

https://doi.org/10.1016/j.ijhydene.2019.11.184

Introduction

Hydrogen (H_2) is an ideal energy carrier because it is clean, abundant and most importantly renewable. It is expected to be the most promising next generation energy carrier replacing the rapidly depleting fossil fuels. As a sustainable energy carrier H_2 has broad range of benefits including reduced greenhouse gas emissions, low-cost and controlled air pollution [1,2]. Though, H_2 appears to be an ideal fuel and the most economical source of renewable energy with the highest energy per mass, it has the lowest energy per unit volume. Thus, the challenge for H_2 based economy respites in developing an efficient H_2 storage technology that could offer high volumetric and gravimetric energy density at an affordable cost [3,4]. The current target by the US Department of Energy (DOE) for H_2 storage is parameterized with the gravimetric density range from 5.5 wt% to 9.5 wt% [5–7]. In addition, for the robust adsorption/desorption mechanism the ideal adsorption energy of H_2 should lie in the range of 0.15–0.6 eV/H_2 [5].

To meet the H_2 storage targets, research groups across the globe have been working on the design of lightweight materials, in particular the porous carbonaceous compound like activated carbon, powdered graphite, carbon nanotubes, and graphene related materials have drawn special attention as efficient storage material over a wide ranges of pressures and temperatures [5–8]. Light weight carbon-based nanostructures; in the form of tubes [2–5], fibers [6–10] and even mechanically milled graphite [8] have been claimed to have a large amount of H_2 uptake. In this context, Ye et al. have reported single-walled carbon nanotubes (SWNTs) achieving 8.0 wt% of H_2 storage at 80 K and above 100 bars of temperature and pressure, respectively [11]. Browning et al. have reported H_2 storage capacity of 6.5 wt% in carbon nano-fibers under 120 bars pressure and at ambient temperature [12]. In these reports the H_2 uptake systems require either high pressure or very low temperature or both that limit the applicability for practical applications.

On the other hand, enhanced H_2 uptake on surface modified carbonaceous materials upon functionalization with alkali (AK), alkaline (ALK), light transition metals (TMs) as well as non-metals (NM) has already been studied extensively [13–16]. The H_2 adsorption energies are reported to be smaller in the case of AK and ALK decoration when compared with TMs decoration. In case of TMs functionalization, strong hybridization between the H $(\sigma-\sigma')$ orbitals with that of low laying empty d-orbitals of TMs leads to Kubas type complexes ensuing enhanced H_2 binding energies [17,18]. However, a major concern with a TM functionalization is the clustering over the host material surfaces, which leads to a lower H_2 storage efficiency. Moreover, due to high molecular weights, the TMs also result into low H_2 gravimetric densities. In this context, by using DFT calculations [2] Sigal et al. have reported that the presence of Ni enhances the H_2 adsorption capacity of graphene sheet, however the lower energy barriers lead to the Ni clusterization, which precludes the practical use for H_2 storage. Therefore, an appropriate approach is the functionalization with lightweight TMs on 2D carbaneous material while avoiding the metal-metal (M-M) clustering effect to achieve high H_2 storage efficiency. In this regard, first-principles computations on Ti-grafted GO predict H_2 storage capacity of 4.9 wt% [19], where the Ti atoms bind strongly to the oxygen sites of the GO sheet preventing Ti–Ti clustering. Hussain et al. have predicted that Li/Ca-doped graphane (hydrogenated graphene: CH) as a potential candidate for H_2 storage, where Li-binding energy on CH is significantly higher than the Li bulk cohesive energy which rules out the possibility of Li–Li cluster formations whereas Ca doped CH reports 6 wt % the H_2 storage capacity [20,21]. By using van der Waal dispersion corrected DFT, the reversible H_2 storage capacity of graphdiyne (GDY) nanosheets functionalized with the lighter metals like Li, Na, K, Ca, Sc and Ti has also been reported elsewhere [22]. Furthermore, DFT calculations by Naqvi et al. have reported high H_2 storage capacity of siligraphene (SiC_7) functionalized with various AK, ALK and TMs while avoiding the (M-M) clustering [23]. The single walled carbon nanotubes (CNT) while functionalized with TiO_2 as well as polylithiated molecules have also been studied with high H_2 storage capacities [24,25].

In another context, it has been reported that the boron doping on graphene (BC-sheet) prevents the M-M clustering effect, while the BC-sheet is being functionalized with both alkaline and transition metals like Ti, Ni, Mg, and Ca for enhanced H_2 storage [26,27]. It has also been reported that the nitrogen doping in graphene (NC-sheets) under functionalization with Pd also enhance the H_2 storage capacity [28,29]. However both B and N-doping on graphene costs high formation energies, which still is a major challenge to deal with [30,31].

Carbonaceous materials like graphitic carbon nitride (g-C_3N_4), which is already enriched with nitrogen and uniform pores is an interesting choice for H_2 storage. The g-C_3N_4 could be an attractive H_2 sorbent for two reasons: firstly, its porous structure allows easy access of H_2 and secondly, the doubly bonded nitrogen at its pore edges provides active sites for either the adsorption of H_2 (chemically and physically), or with functionalization with metal dopants [32–34]. Using DFT level simulation several groups have predicted the H_2 storage capacity of Li/Ti/Pd functionalized g-C_3N_4 sheet [35–37].

Motivated by the interesting properties of two-dimensional g-C_3N_4 sheet, here by using van der Waals corrected (DFT-D) simulation; we have investigated the structural, electronic and H_2 uptake propensity of g-C_3N_4 sheet functionalized with TMs like Sc, Ti, Ni and V and their respective dimer, Sc_2, Ti_2, Ni_2 and V_2.

Methodology

The calculations throughout this project were carried out on the basis of spin polarized density functional theory (DFT) by using the Vienna ab initio simulation package (VASP) [38,39]. For electrons, the exchange and correlation interaction parts were treated within generalized gradient approximation (GGA) by taking Perdew–Bruke–Ernzerhof (PBE) functional [40]. The interactions between electrons and the core were described by the projector augmented wave (PAW) approach, which treats the electronic states of C (s2p2), N (s2p1), Sc (3p4s3d), Ti (s2p1), Ni () and V (s2p2) as valence states. To

describe the interaction of H_2 to g-C_3N_4 sheets, which are weakly interacting systems, the conventional GGA-PBE would underestimate the binding energies especially for these hydrogen-bonded systems [41]. For such systems one needs to incorporate the van der Waals corrections as implemented in DFT-D within VASP, which takes care of the non-local, and long-ranged van der Waals (vdW) forces. Here, we have implemented the DFT-D3 method as prescribed by Grimme [42], to accurately determine the electronic structures and energetics of the studied systems.

We have modeled a 3 × 3 × 1 supercell of g-C_3N_4, which consisted of 24 C and 32 N atoms, by using periodic boundary conditions. A vacuum of 15 Å is maintained along the perpendicular direction of the sheet to avoid the coupling effect with the periodic structures. For the plane wave basis set the energy cutoff was optimized to be 500 eV. To obtain the ground state geometries, all the structures are optimized without any symmetry constraints by using the conjugate gradient (CG) algorithm. The atomic positions and lattice parameters are optimized with energy convergence criterion of 10^{-5} eV between two ionic steps and the forces are converged with the maximum force on each atom to be 0.001-eV/Å. For the total energy calculations the Brillouin zone is sampled in the k-space within Monkhorst-Pack scheme by a dense grid of 5 × 5 × 1 [43].

The binding energy E_b of the metals (Ti, Sc, Ni, V) to the g-C_3N_4 sheet is calculated as follows,

$$E_b = E(DFT)_{g-C_3N_4-M} - \left[E(DFT)_{g-C_3N_4} + nE\left(DFT\right)_M\right] \quad (1)$$

Here, $E(DFT)_{g-C_3N_{4-M}}$ and $E(DFT)_{g-C_3N_4}$ represents the Kohn-Sham (KS) DFT energy of g-C_3N_4 sheet functionalized with metals M (Ti, Sc, Ni, V) and that of pristine g-C_3N_4 sheet, respectively. Here $E(DFT)_M$ represents the energy of metal atoms and n presents the number of functionalized atoms.

The H_2 adsorption energy (E_{ads}) to the functionalized sheet is calculated as follows.

$$E_{ads} = \left\{E_{g-C_3N_4-M-nH_2} - \left[E_{g-C_3N_4-M} + nE_{H_2}\right]\right\}/n \quad (2)$$

Here, $E_{g-C_3N_4-M-nH_2}$ is the energy of hydrogenated g-C_3N_4 sheet functionalized with metals M, $E_{g-C_3N_4-M}$ is the energy of functionalized g-C_3N_4 sheet and E_{H_2} and n presents the energy of H_2 and number of H_2 molecules respectively.

Result and discussion

The optimized structure of the g-C_3N_4 sheet having two types of C–N bonds of bond length 1.39 and 1.47 Å and with N–C–N and C–N–C bond angles as 122.0° and 119.0° respectively is presented in Fig. 1(a). Fig. 1(b) shows the spin-polarized deinsity of states (SPDOS) of pristine g-C_3N_4 shows non-magnetic behavior with a band-gap of E_g of 1.2 eV. The underestimation in E_g compared to the reported E_g of 2.3 eV [44] is due to the shortcoming of the PBE functional to estimate the accurate E_g.

Since the pristine g-C_3N_4 has weak affinity towards H_2, it is functionalized with the dopants M (Sc, Ti, Ni, V) and their corresponding dimers M_2 (Sc_2, Ti_2, Ni_2, V_2). The most stable configurations of the M dopants on g-C_3N_4 were investigated by exploring all available binding sites like bigger hole (B-hole), smaller hole (s-hole), carbon top (C-top), nitrogen top (N-top), C–N bridge. As the M functionalization at B-hole was energetically more favorable as compared to all other configurations, hereafter functionalization at B-hole systems are only discussed for structural, electronic and H_2 storage applications. The optimized structures of Sc, Ti, Ni, and V functionalized g-C_3N_4 (g-C_3N_4@M) are shown in Fig. 2 (a), 3 (a), 4 (a) and 5 (a), respectively. Most of the g-C_3N_4@M sheets retain their planner structure, with slight structural rearrangements. The binding energies (E_b) values of the dopants (M) and dimers (M_2) over g-C_3N_4 have been calculated by using the relation (1) and the results are summarized in Table 1. The calculated E_b values for Sc, Ti and Ni to g–C_3N_4–sheet are much higher than their binding to graphene, graphdiyne and boron carbide sheets [13,15].

For an efficient and reversible binding mechanism, E_b of M on g-C_3N_4 should be higher than the corresponding M-M cohesive energies (E_c), i.e. [$E_b/E_c > 1$]. In the case of $E_b/E_c < 1$, the M-M clustering would prevent binding of M to g-C_3N_4. A

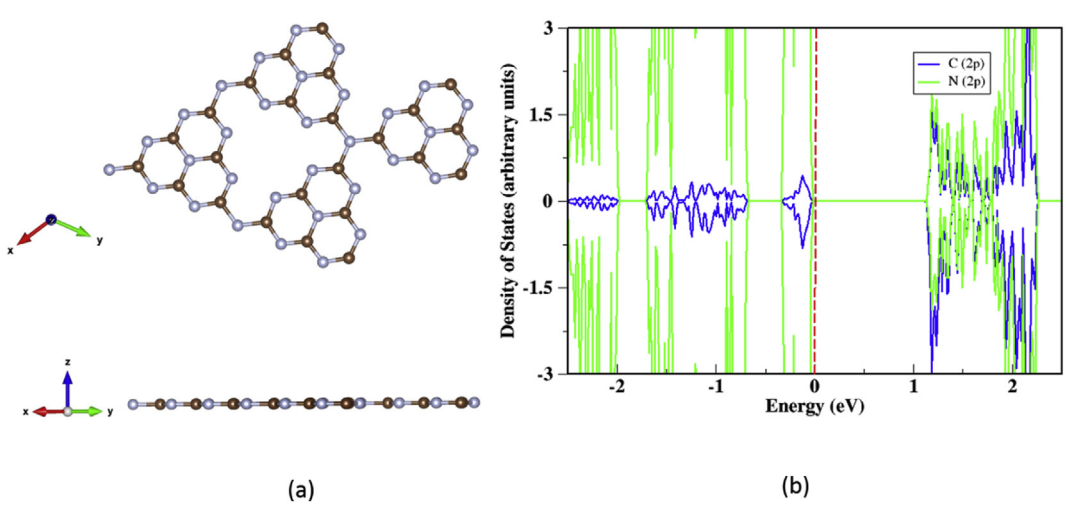

Fig. 1 – (a) Ground state structure of g-C_4N_4 Grey: C, Golden brown: N (b) spin-polarized density of states (SPDOS) of g-C_3N_4. (For interpretation of the references to color in this figure legend, the reader is referred to the Web version of this article.)

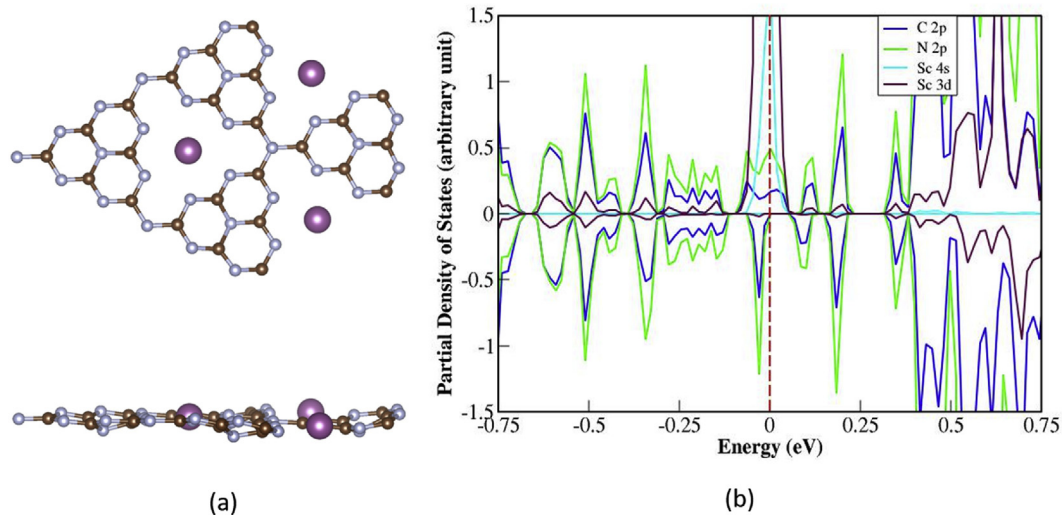

Fig. 2 – (a) Ground state structure and (b) spin polarized density of states (SPDOS) of g-C_3N_4@Sc. Grey: C, Golden brown: N, Purple: Sc. (For interpretation of the references to color in this figure legend, the reader is referred to the Web version of this article.)

reasonably high M-M distance also ensures the uniform distribution of M over g-C_3N_4 and each M (or M_2) would act as an individual active site for the H_2 adsorption.

The electronic properties of Sc, Ti, Ni and V functionalized g-C_3N_4 are depicted in the SPDOS plots as Figs. 2(b), 3(b), 4(b) and 5(b), respectively. In all the four g-C_3N_4@M systems there is a transition from semiconducting state to metallic state. In the case of g-C_3N_4@Sc, the SPDOS plot depicts a strong hybridization between *Sc-3d* and *Sc-4s* states with both *C-2p* and *N-2p* states at the Fermi level. The *Sc-4s* states dominate at the Fermi level. With Sc doping, there is shift for both spin up *C-2p* and *N-2p* states from Fermi to conduction band region. Bader analysis, revels a charge transfer of 0.3*e* from Sc to the g-C_3N_4. The bulk portion of this transferred charged was accumulated by the N atoms, which are in the close vicinity of the dopants Sc. This transfer of charge from spin down states of *Sc-4d* makes the Sc as a cationic entity (Sc^+).

From the SPDOS plot in Fig. 3 (b) the hybridization between *Ti-3d* states with that of *C-2p* and *N-2p* states near the Fermi energy explains the strong binding of Ti to the g-C_3N_4 (Table 1). Bader analysis revels a significant charge transfer from the Ti atoms, which was mainly accumulated over the N-atoms of g-C_3N_4@Ti sheet. Similarly, the SPDOS plot in Fig. 4 (b) of g-C_3N_4@Ni sheet depicts *Ni-3d* states being hybridized with that of *C-2p* and *N-2p* states. Bader analysis shows that, similar to Sc and Ti, the Ni dopants lose their electronic charge to the g-C_3N_4. The charge clouds are getting accumulated to the spin-down states of *Ni-3d* as well as *N-2p* states as evident from the SPDOS plot at the Fermi level. In case of g-C_3N_4@V, the SPDOS plot depicts the hybridization between *V-3d* states with that of *C-2p* and *N-2p* states at the Fermi level.

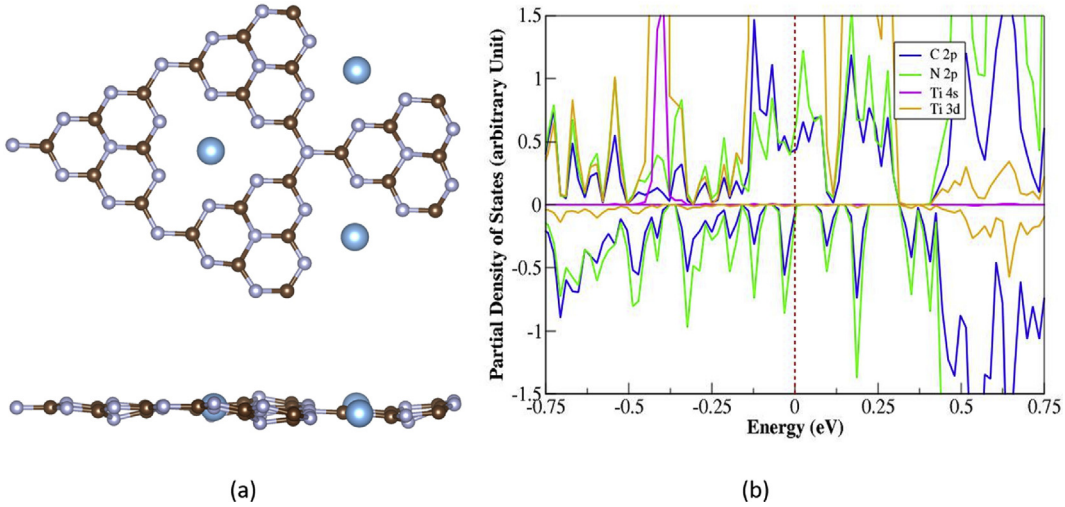

Fig. 3 – (a) Ground state structure and (b) spin polarized density of states (SPDOS) of g-C_3N_4@Ti. Grey: C, Golden brown: N, Cyan: Ti. (For interpretation of the references to color in this figure legend, the reader is referred to the Web version of this article.)

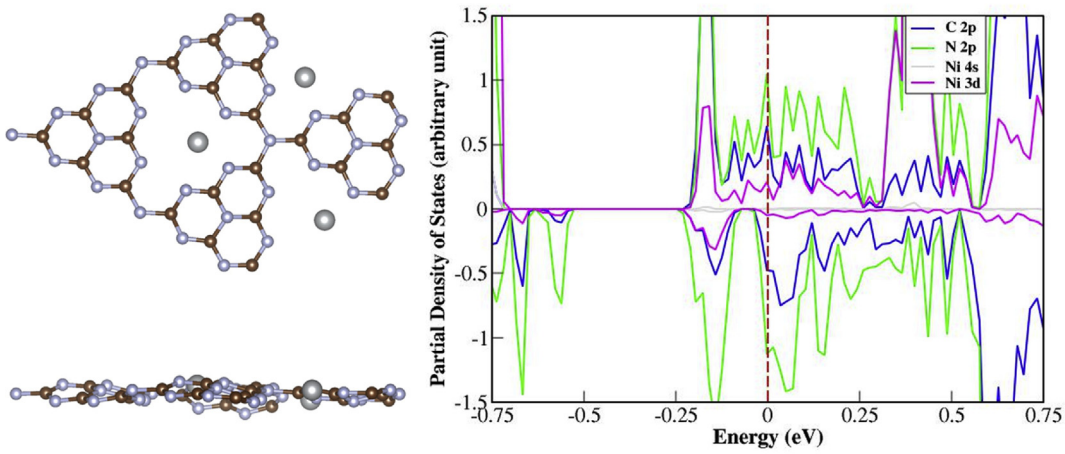

(a) (b)

Fig. 4 – (a) Ground state structure and (b) spin polarized density of states (SPDOS) of g-C_3N_4@Ni. Grey: C, Golden brown: N, Ash grey: Ni. (For interpretation of the references to color in this figure legend, the reader is referred to the Web version of this article.)

Table 1 – Binding energies of M and M_2 dopants on g-C_3N_4 nanosheets. The experimental cohesive energies are also given.

System	M-M Bulk cohesive energy (E_c) eV	Binding energy (E_b) per M (eV)	Binding energy (E_b) per (M_2) (eV)
Sc	−3.90	−7.26	−8.36
Ti	−4.85	−6.97	−10.67
Ni	−4.44	−3.01	−4.43
V	−5.31	−8.27	−6.42

To ensure the thermal stability of functionalized g-C_3N_4@M sheets we have performed ab initio molecular dynamics (*AIMD*) simulations on all the four sheets by using Nose-thermostat algorithm at 400 K for 6 ps with a time step of 1fs. The g-C_3N_4@M sheets are predicted to remain stable without any structural deformation as evident from a small variation in the energies as shown in Fig. 6.

The optimized structures of g-C_3N_4@M_2 are presented in Figs. 7(a), 8(a), 9(a) and 10 (a) respectively, and the E_b values are presented in Table 1. In case of Sc_2 and Ti_2 functionalization, the g-C_3N_4 maintains the planner structure however small buckling is observed in case of Ni_2 and V_2. Compare to single atom functionalization, the dimers are found to have stronger binding to the g-C_3N_4

Similar to the case of g-C_3N_4@M, we have studied the electronic properties of g-C_3N_4@M_2. In case of g–C_3N_4–Sc_2, from the SPDOS plots in Fig. 7 (b) it is evident that *C-2p* states strongly hybridizes with that of *Sc-3d* and *Sc-4s* states, which are mostly dominating near the Fermi region. Bader analysis shows that both the Sc in the g-C_3N_4@Sc_2 loses charge of 0.5e each and act individual cationic entity. The SPDOS plot of g-C_3N_4@Ti_2 sheet in Fig. 8 (b) shows the hybridization between

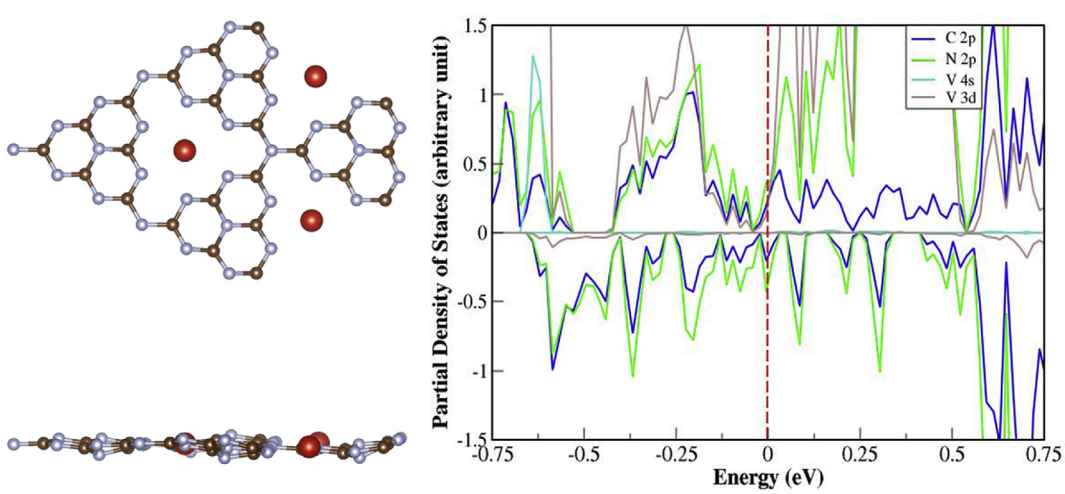

(a) (b)

Fig. 5 – (a) Ground state structure and (b) spin polarized density of states (SPDOS) of g-C_3N_4@V. Grey: C, Golden brown: N, Red: V. (For interpretation of the references to color in this figure legend, the reader is referred to the Web version of this article.)

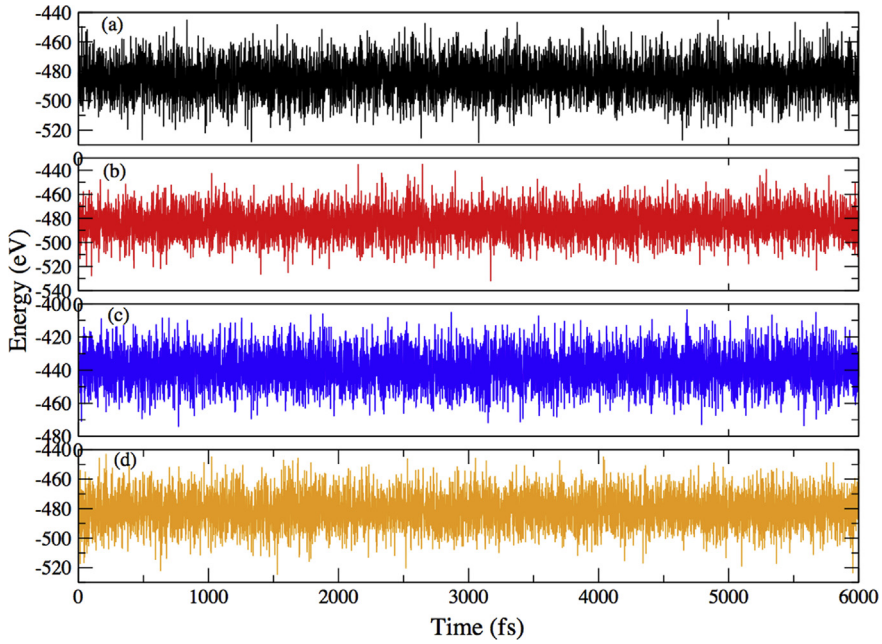

Fig. 6 – AIMD plots of (a) g-C_3N_4@Sc, (b) g-C_3N_4@Ti, (c) g-C_3N_4@Ni, (d) g-C_3N_4@V. The structures of g–C_3N_4–M having high thermal stability and with dopants in cationic states are capable to anchor multiple H_2 molecules. Motivated by the strong binding of single M on the g-C_3N_4, we have studied the binding mechanism of dimers M_2 (Sc_2, Ti_2, Ni_2, V_2) on g-C_3N_4 sheet. It would increase the active binding sites for further H_2 adsorption and enhance the storage capacity.

C-2p and *N-2p* states with that of *Ti-3d* states and there is charge transfer to the spin-up *C-2p* states. Both the Ti atoms in g-C_3N_4@Ti_2 configuration lose a charge of 0.6 e each. In the case of g-C_3N_4@Ni_2 the SPDOS plot in Fig. 9 (b) shows the hybridization between *Ni-4s* and *N-3d* states with that of *C-2p* and *N-2p* states near the Fermi level. There is a charge accumulation in the spin-down states of *Ni-3d* states, which is also confirmed by bader charge analysis. Each Ni of g-C_3N_4@Ni_2 loses a charge of 0.7e each. From the SPDOS plot of g-C_3N_4@V_2, the valence band region depicts hybridization between *V-3d* with that of *C-2p* states. It is found that the each V in g-C_3N_4@V_2 loses charge of 0.4 e each, which is accumulated by the N atoms of g-C_3N_4.

Hydrogenation of M functionalized g-C_3N_4

This section emphasizes on the adsorption of H_2 to each of the g-C_3N_4@M as well as g-C_3N_4@M_2 sheets. As the dopants M

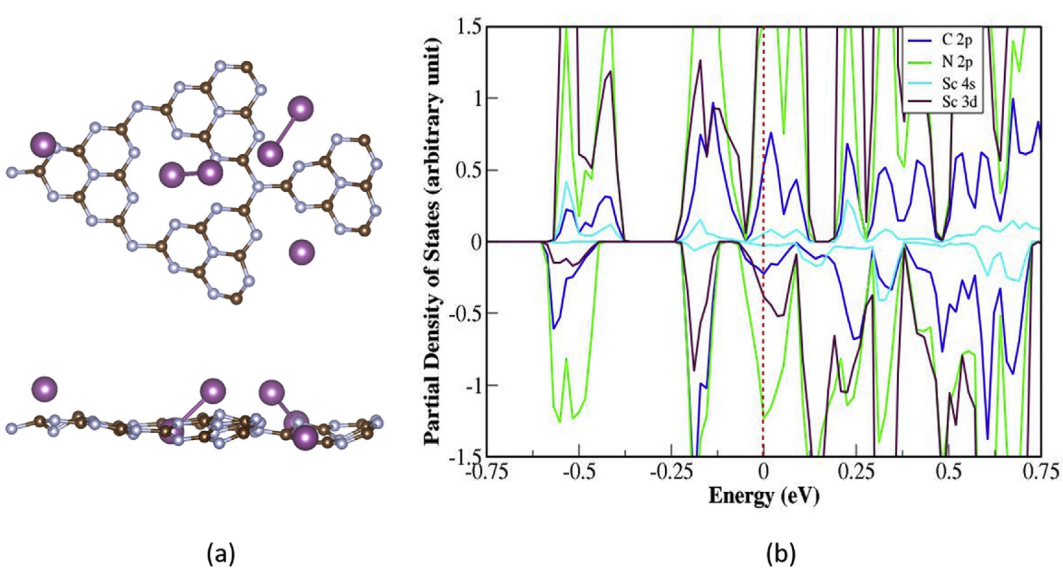

Fig. 7 – (a) Ground state structure and (b) spin polarized density of states (SPDOS) of g-C_3N_4@Sc_2. Grey: C, Golden brown: N, purple: Sc. (For interpretation of the references to color in this figure legend, the reader is referred to the Web version of this article.)

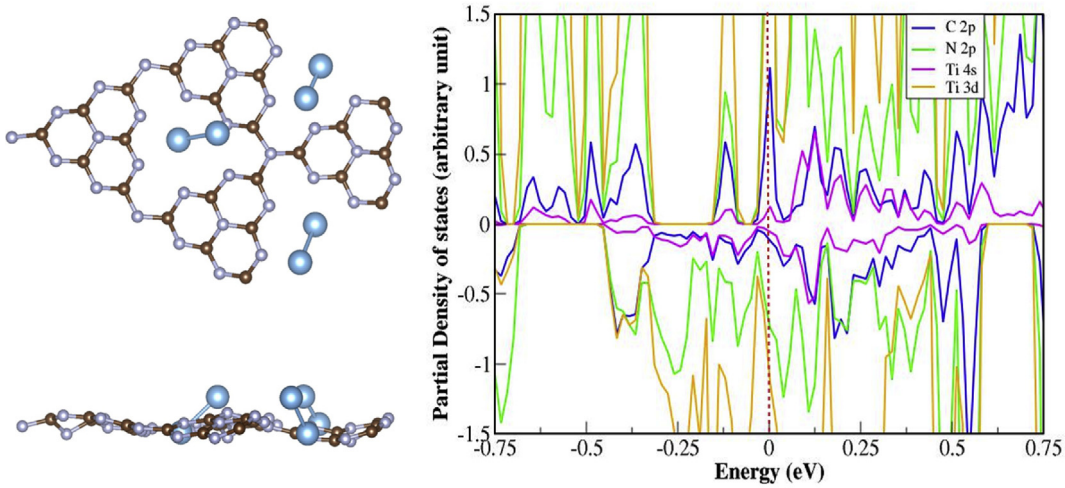

(a) (b)

Fig. 8 – (a) Ground state structure and (b) spin polarized density of states (SPDOS) of g-C_3N_4@Ti_2. Grey: C, Golden brown: N, Cyan: Ti. (For interpretation of the references to color in this figure legend, the reader is referred to the Web version of this article.)

and M_2 are in cationic states, by donating a portion of their charges to the g-C_3N_4, and are able to polarize the adsorbing H_2 molecules and bind them through electrostatic attractions. The polarization alters the H–H bond length of H_2 in all the metal decorated g-C_3N_4 systems. For example in case of C_3N_4@Sc-6H_2, the H–H bond lengths elongates from 0.75 to 0.78 Å, whereas in C_3N_4@Ti–6H_2, the average H–H bonds elongates further to 0.90 Å. Similarly, C_3N_4@Ni and C_3N_4@V lengths the average H–H bonds to 0.86 and 0.84 Å, respectively. We have studied the adsorption mechanism of H_2 molecules on each of the M and M_2 simultaneously. The hydrogenation process takes place in step-wise manner. First a single H_2 is introduced on each M and the systems are allowed to optimize completely. After attaining structural optimization with single H_2, the second H_2 is introduced to the g-C_3N_4@M – H_2 and the system is again relaxed completely. This process continues until the systems reach to their saturation, that is a stage when the further exposure of H_2 are repelled due to the existing polarized H_2 molecules. All the hydrogenated systems of M (Sc, Ti, Ni, V) functionalized g-C_3N_4 (g–C_3N_4–M and g-C_3N_4@M_2), with one and two-sided coverage are shown in Figs. 11 and 12 respectively. We have concluded that a maximum of 6H_2 and 12H_2 molecules could be adsorbed on one and two-sided coverage of g–C_3N_4–M, respectively. The E_{ads} values of H_2 to g–C_3N_4–M sheets are presented in Table 2. We can find that in case of M functionalization, the E_{ads} values are in the range of 0.1–0.3 eV/H_2, which are on the lower sides. However in case of M_2 functionalization g-C_3N_4 sheets (g–C_3N_4–M_2) a maximum of 12H_2 molecules could be adsorbed with E_{ads}

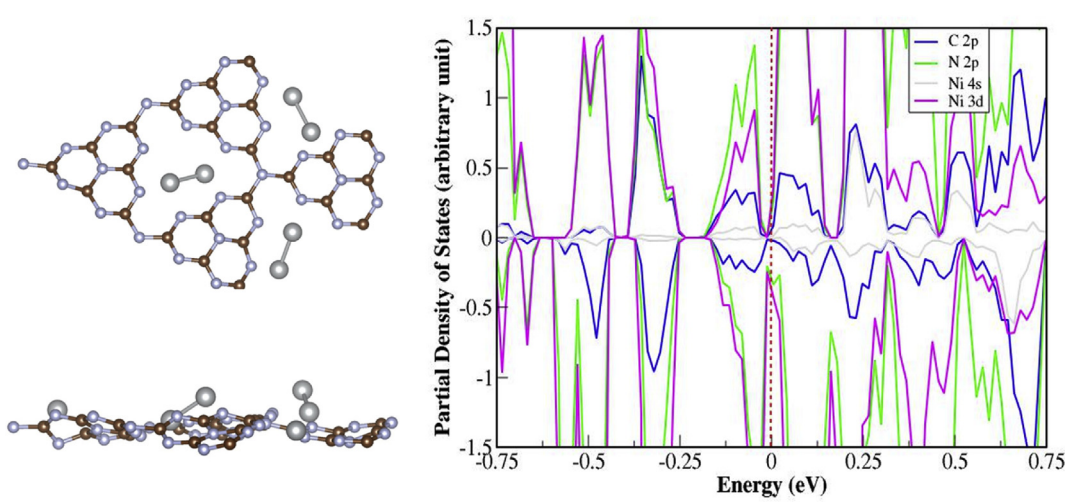

(a) (b)

Fig. 9 – (a) Ground state structure and (b) spin polarized density of states (SPDOS) of g-C_3N_4@Ni_2. Grey: C, Golden brown: N, purple: Sc. (For interpretation of the references to color in this figure legend, the reader is referred to the Web version of this article.)

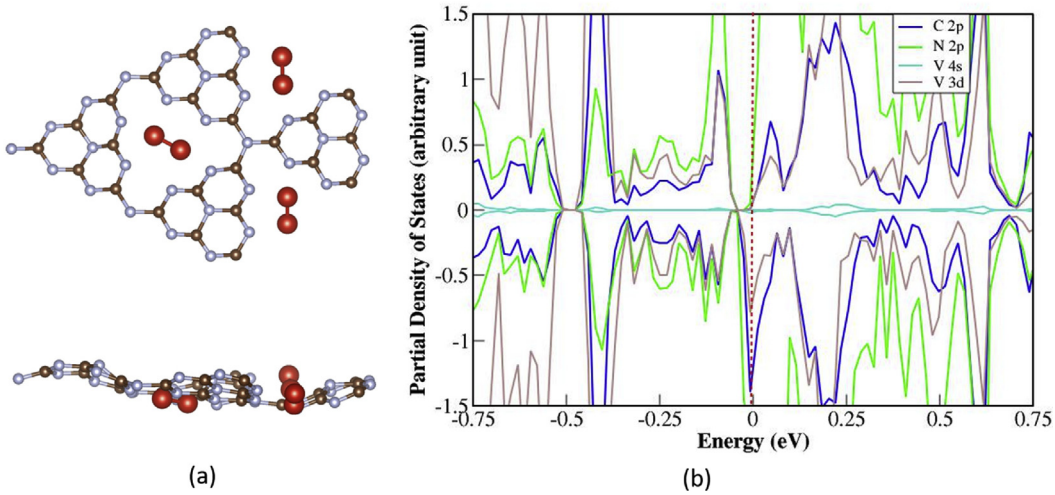

Fig. 10 – (a) Ground state structure and (b) spin polarized density of states (SPDOS) of g-C_3N_4@Sc_2. Grey: C, Golden brown: N, Red: V. (For interpretation of the references to color in this figure legend, the reader is referred to the Web version of this article.)

values in the range of 0.6–0.9 eV/H_2, which are very promising. Similar to the cases of hydrogenated g–C_3N_4–M, there is an elongation in H–H bonds in case of H_2 adsorbed g–C_3N_4–M_2 systems. Here the H–H elongation is more pounced as compared to the g–C_3N_4–M. Ground state structures of hydrogenated g–C_3N_4–M_2 are shown as Fig. 11(a–d). Tremendous improvement in H_2 adsorption over g–C_3N_4–M_2 clearly indicate that the introduction of selected M dopants, either monomers or dimers, transforms the g-C_3N_4 sheets from non-responsive to efficient H_2 storage mediums.

Furthermore, to estimate the desorption conditions of the adsorbed H_2 molecules on g–C_3N_4–M and g–C_3N_4–M_2, we have calculated the desorption temperatures by using van't Hoff equation as given below [45].

$$T_d = \frac{E_b}{k_B}\left(\frac{\Delta S}{R}\right)^{-1}$$

In this relation.

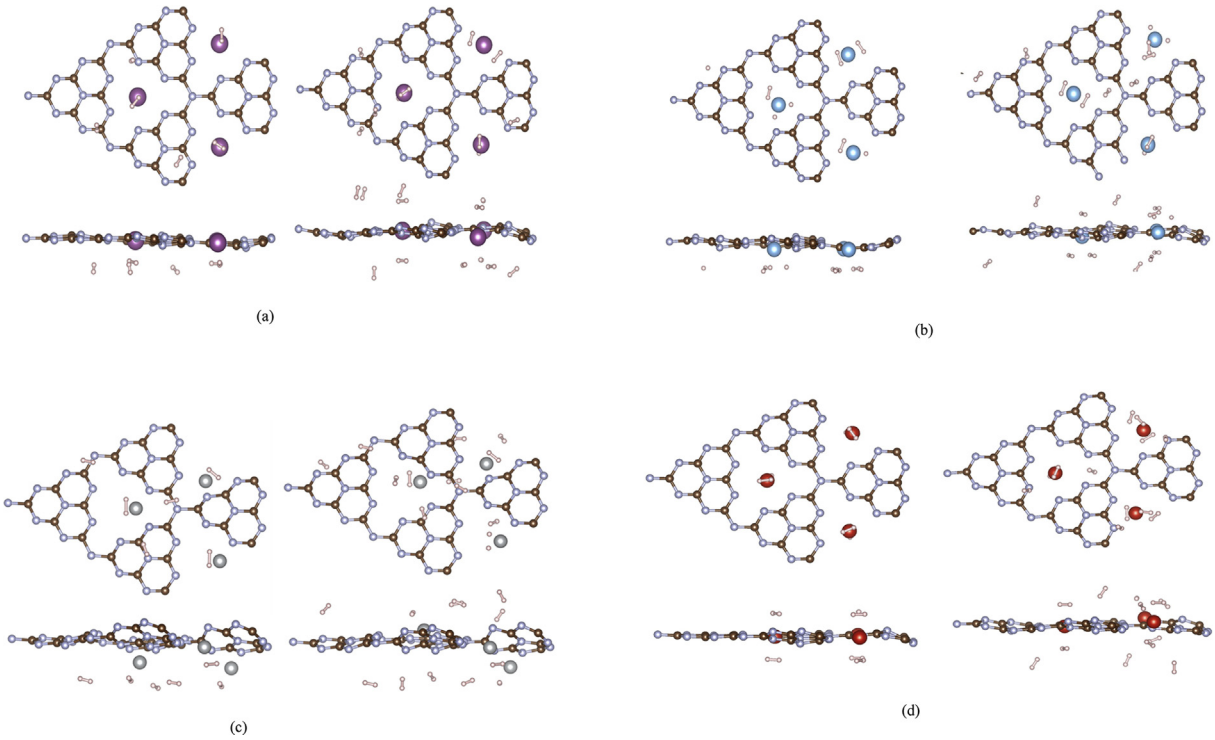

Fig. 11 – (a), (b), (c), (d) Top and side view of optimized hydrogenated g–C_3N_4–M sheets with M (Sc, Ti, Ni, V). Grey: C, Golden brown: N, Purple: Sc, Cyan: Ti, Grey: Ni and Red: V. (For interpretation of the references to color in this figure legend, the reader is referred to the Web version of this article.)

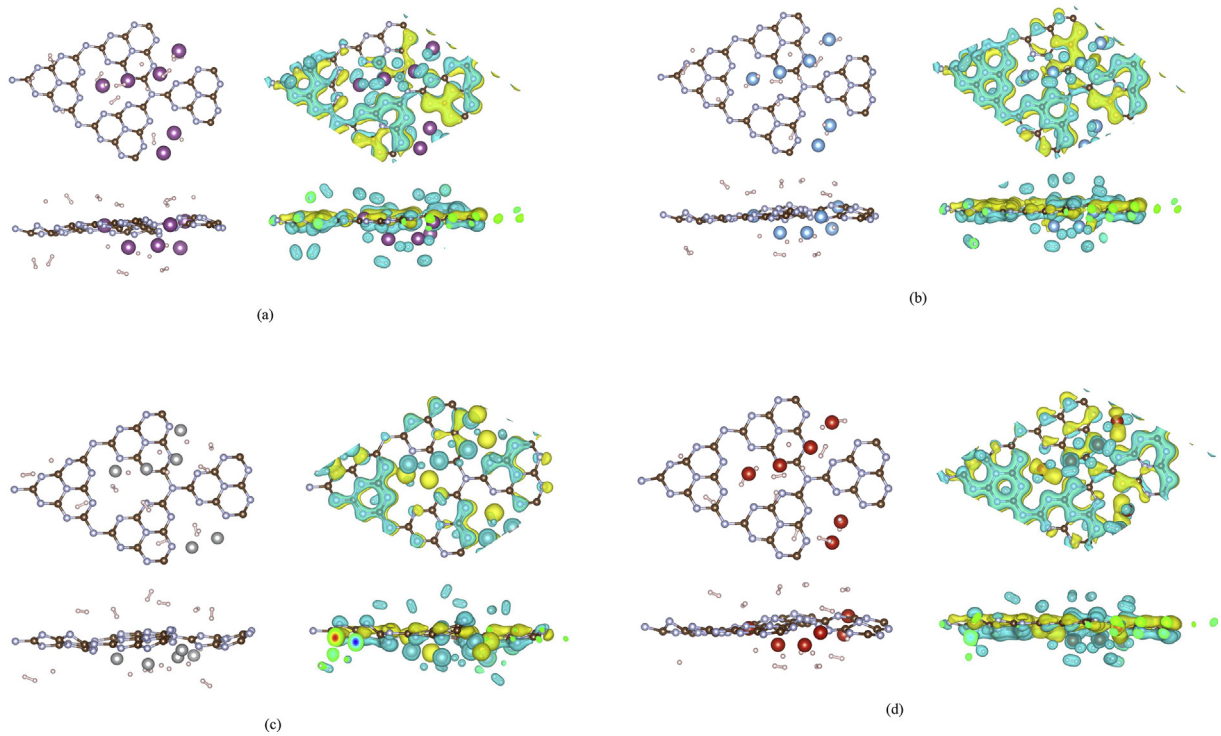

Fig. 12 – (a), (b), (c) (d), {left panel} Top and side view of optimized hydrogenated g–C_3N_4–M2 sheets with M (Sc, Ti, Ni, V) and {right panel} the corresponding isosurface charge density plots. Grey: C, Golden brown: N, Purple: Sc, Cyan: Ti, Grey: Ni and Red: V. Sea-green: charge depletion and Yellow: charge accumulation. (For interpretation of the references to color in this figure legend, the reader is referred to the Web version of this article.)

Table 2 – Van der Waals corrected adsorption energies per H_2 molecules of g-C_3N_4@M and g-C_3N_4@M_2 and the corresponding desorption temperatures.

System	Binding Energy per H_2 (eV)			Desorption Temperature (K)		
	Single-Side	Double-Side	Dimers	Single-Side	Double-Side	Dimers
Sc	−0.13	−0.21	−0.69	166	269	883
Ti	−0.02	−0.16	−0.93	25.6	205	1190
Ni	−0.38	−0.27	−0.46	486	345	589
V	−0.12	−0.05	−0.28	154	64	358

E_b = Van der Waals corrected H_2 adsorption energies (in J per H_2 molecule)
R = Universal gas constant
kB = Boltzmann constant
ΔS = Change of H_2 entropy from gas to liquid phase (75.44 J/mol/K)

Summary

In summary, by using spin-polarized DFT-D2 level of simulation the structural, electronic properties and the charge transfer and H_2 adsorption mechanism of metal functionalized g-C_3N_4 sheets was explored. Our calculations predict that g-C_3N_4 binds fairly to metals dopants like Sc, Ti, Ni and V and even more strongly to their respective dimer structures, which is much higher than the dopant's experimental cohesive energies. Therefore a uniform coverage effect is possible to be achieved for these metals dopants on g-C_3N_4 while avoiding metal-metal clustering effect. The AIMD simulations at 400 K confirm the thermal stabilities of all the four metal functionalized g-C_3N_4 sheets. Bader charge analysis reveals a significant charge transfer from the metal dopants to the N atoms of the g-C_3N_4 sheet. As a result the metal dopants act as cationic entity having high affinity towards the H_2 molecules while polarizing them. Compare to monomers, dimers functionalization to g-C_3N_4 sheet are found to be more promising for H_2 storage as binding energy per H_2 molecule falls in the range of 0.6–0.9 eV/H_2.

Acknowledgement

PP is indebted to the CENCON for financial support. RA would like to thanks the Carl Tryggers Stiftelse for Vetenskaplig Forskning (CTS) and Swedish Research Council (VR) for financial support. SNIC and SNAC are acknowledged for

providing the computing facilities. AK acknowledges an Australian Research Council (ARC) Future Fellowship (FT170100373).

Appendix A. Supplementary data

Supplementary data to this article can be found online at https://doi.org/10.1016/j.ijhydene.2019.11.184.

REFERENCES

[1] Tollefson J. Hydrogen vehicles: fuel of the future? Nature 2010;464:1262–4. https://doi.org/10.1038/4641262a.
[2] Sigal A, Rojas MI, Leiva EPM. Interferents for hydrogen storage on a graphene sheet decorated with nickel: a DFT study. Int J Hydrogen Energy 2011;36:3537–46. https://doi.org/10.1016/J.IJHYDENE.2010.12.024.
[3] Bénard P, Chahine R. Storage of hydrogen by physisorption on carbon and nanostructured materials. Scr Mater 2007;56:803–8. https://doi.org/10.1016/J.SCRIPTAMAT.2007.01.008.
[4] Burress J, Kraus M, Beckner M, Cepel R, Suppes G, Wexler C, et al. Hydrogen storage in engineered carbon nanospaces. Nanotechnology 2009;20:204026. https://doi.org/10.1088/0957-4484/20/20/204026.
[5] Liu C, Fan YY, Liu M, Cong HT, Cheng HM, Dresselhaus MS. Hydrogen storage in single-walled carbon nanotubes at room temperature. Science 1999;286:1127–9. https://doi.org/10.1126/science.286.5442.1127 (80-).
[6] Chambers A, Park C, Baker RTK, Rodriguez NM. Hydrogen storage in graphite nanofibers. J Phys Chem B 1998;102:4253–6. https://doi.org/10.1021/jp980114l.
[7] Chen Wu, Lin Tan. High H2 uptake by alkali-doped carbon nanotubes under ambient pressure and moderate temperatures. Science 1999;285:91–3.
[8] Cheng H-M, Liu C, Fan YY, Li F, Su G, Cong H, et al. Synthesis and hydrogen storage of carbon nanofibers and single-walled carbon nanotubes, vol. 91; 2000. p. 306–10.
[9] Ahn CC, Ye Y, Ratnakumar BV, Witham C, Bowman RC, Fultz B. Hydrogen desorption and adsorption measurements on graphite nanofibers. Appl Phys Lett 1998;73:3378–80. https://doi.org/10.1063/1.122755.
[10] Dillon AC, Jones KM, Bekkedahl TA, Kiang CH, Bethune DS, Heben MJ. Storage of hydrogen in single-walled carbon nanotubes. Nature 1997;386:377–9. https://doi.org/10.1038/386377a0.
[11] Ye Y, Ahn CC, Witham C, Fultz B, Liu J, Rinzler AG, et al. Hydrogen adsorption and cohesive energy of single-walled carbon nanotubes. Appl Phys Lett 1999;74:2307–9. https://doi.org/10.1063/1.123833.
[12] Browning DJ, Gerrard ML, Lakeman JB, Mellor IM, Mortimer RJ, Turpin MC. Studies into the storage of hydrogen in carbon nanofibers: proposal of a possible reaction. Mechanism 2002. https://doi.org/10.1021/NL015576G.
[13] Bodrenko IV, Avdeenkov AV, Bessarabov DG, Bibikov AV, Nikolaev AV, Taran MD, et al. Hydrogen storage in aromatic carbon ring based molecular materials decorated with alkali or alkali-earth metals. J Phys Chem C 2012. https://doi.org/10.1021/jp305324p.
[14] Wu M, Gao Y, Zhang Z, Zeng XC. Edge-decorated graphene nanoribbons by scandium as hydrogen storage media. Nanoscale 2012. https://doi.org/10.1039/c2nr11257d.
[15] Naqvi SR, Hussain T, Panigrahi P, Luo W, Ahuja R. Manipulating energy storage characteristics of ultrathin boron carbide monolayer under varied scandium doping. RSC Adv 2017. https://doi.org/10.1039/c6ra24890j.
[16] Ramos-Castillo CM, Reveles JU, Cifuentes-Quintal ME, Zope RR, De Coss R. Ti4- and Ni4-doped defective graphene nanoplatelets as efficient materials for hydrogen storage. J Phys Chem C 2016. https://doi.org/10.1021/acs.jpcc.5b12711.
[17] Kubas GJ. Metal-dihydrogen and σ-bond coordination: the consummate extension of the Dewar-Chatt-Duncanson model for metal-olefin π bonding. J Organomet Chem 2001. https://doi.org/10.1016/S0022-328X(01)01066-X.
[18] Kubas GJ. Fundamentals of H 2 binding and reactivity on transition metals underlying hydrogenase function and H 2 production and storage. Chem Rev 2007. https://doi.org/10.1021/cr050197j.
[19] Wang L, Lee K, Sun YY, Lucking M, Chen Z, Zhao JJ, et al. Graphene oxide as an ideal substrate for hydrogen storage. ACS Nano 2009. https://doi.org/10.1021/nn900667s.
[20] Hussain T, De Sarkar A, Ahuja R. Strain induced lithium functionalized graphane as a high capacity hydrogen storage material. Appl Phys Lett 2012. https://doi.org/10.1063/1.4751249.
[21] Hussain T, Pathak B, Ramzan M, Maark TA, Ahuja R. Calcium doped graphane as a hydrogen storage material. Appl Phys Lett 2012. https://doi.org/10.1063/1.4710526.
[22] Panigrahi P, Dhinakaran AK, Naqvi SR, Gollu SR, Ahuja R, Hussain T. Light metal decorated graphdiyne nanosheets for reversible hydrogen storage. Nanotechnology 2018;29. https://doi.org/10.1088/1361-6528/aac84c.
[23] Naqvi SR, Hussain T, Luo W, Ahuja R. Metallized siligraphene nanosheets (SiC7) as high capacity hydrogen storage materials. Nano Res 2018. https://doi.org/10.1007/s12274-017-1954-z.
[24] Lavanya R, Surya VJ, Lakshmi I, Iyakutti K, Vasu V, Mizuseki H, et al. Hydrogen storage in TiO_2 functionalized (10, 10) single walled carbon nanotube (SWCNT) – first principles study. Int J Hydrogen Energy 2014;39:4973–80. https://doi.org/10.1016/J.IJHYDENE.2014.01.048.
[25] Panigrahi P, Naqvi SR, Hankel M, Ahuja R, Hussain T. Enriching the hydrogen storage capacity of carbon nanotube doped with polylithiated molecules. Appl Surf Sci 2018. https://doi.org/10.1016/j.apsusc.2018.02.040.
[26] Nachimuthu S, Lai PJ, Leggesse EG, Jiang JC. A first principles study on boron-doped graphene decorated by Ni-Ti-Mg atoms for enhanced hydrogen storage performance. Sci Rep 2015. https://doi.org/10.1038/srep16797.
[27] Beheshti E, Nojeh A, Servati P. A first-principles study of calcium-decorated, boron-doped graphene for high capacity hydrogen storage. Carbon N Y 2011. https://doi.org/10.1016/j.carbon.2010.12.023.
[28] Parambhath VB, Nagar R, Ramaprabhu S. Effect of nitrogen doping on hydrogen storage capacity of palladium decorated graphene. Langmuir 2012. https://doi.org/10.1021/la301232r.
[29] Vinayan BP, Sethupathi K, Ramaprabhu S. Hydrogen storage studies of palladium decorated nitrogen doped graphene nanoplatelets. J Nanosci Nanotechnol 2012. https://doi.org/10.1166/jnn.2012.4539.
[30] Panchakarla LS, Subrahmanyam KS, Saha SK, Govindaraj A, Krishnamurthy HR, Waghmare UV, et al. Synthesis, structure, and properties of boron- and nitrogen-doped graphene. Adv Mater 2009. https://doi.org/10.1002/adma.200901285.
[31] Wu M, Cao C, Jiang JZ. Light non-metallic atom (B, N, O and F)-doped graphene: a first-principles study. Nanotechnology 2010;21:505202. https://doi.org/10.1088/0957-4484/21/50/505202.
[32] Zou LR, Huang GF, Li DF, Liu JH, Pan AL, Huang WQ. A facile and rapid route for synthesis of g-C3N4 nanosheets with

high adsorption capacity and photocatalytic activity. RSC Adv 2016. https://doi.org/10.1039/c6ra20514c.

[33] Nair AAS, Sundara R, Anitha N. Hydrogen storage performance of palladium nanoparticles decorated graphitic carbon nitride. Int J Hydrogen Energy 2015. https://doi.org/10.1016/j.ijhydene.2014.12.065.

[34] Tang X, Gu Y, Kou L. Theoretical investigation of calcium-decorated β_{12}boron sheet for hydrogen storage. Chem Phys Lett 2018. https://doi.org/10.1016/j.cplett.2018.02.022.

[35] Hussain T, Hankel M, Searles DJ. Computational evaluation of lithium-functionalized carbon nitride (g-C6N8) monolayer as an efficient hydrogen storage. Material. J Phys Chem C 2016. https://doi.org/10.1021/acs.jpcc.6b06182.

[36] Wei J, Huang C, Wu H, Kan E. High-capacity hydrogen storage in Li-adsorbed g-C3N4. Mater Chem Phys 2016;180:440–4. https://doi.org/10.1016/J.MATCHEMPHYS.2016.06.028.

[37] Zhang W, Zhang Z, Zhang F, Yang W. Ti-decorated graphitic-C 3 N 4 monolayer: a promising material for hydrogen storage. Appl Surf Sci 2016. https://doi.org/10.1016/j.apsusc.2016.06.019.

[38] Kresse G, Hafner J. *Ab initio* molecular dynamics for liquid metals. Phys Rev B 1993. https://doi.org/10.1103/PhysRevB.47.558.

[39] Kresse G, Hafner J. Ab initio molecular-dynamics simulation of the liquid-metalamorphous- semiconductor transition in germanium. Phys Rev B 1994. https://doi.org/10.1103/PhysRevB.49.14251.

[40] Perdew JP, Burke K, Ernzerhof M. Generalized gradient approximation made simple. Phys Rev Lett 1996;77:3865–8. https://doi.org/10.1103/PhysRevLett.77.3865.

[41] Blöchl PE. Projector augmented-wave method. Phys Rev B 1994;50:17953–79. https://doi.org/10.1103/PhysRevB.50.17953.

[42] Grimme S. Semiempirical GGA-type density functional constructed with a long-range dispersion correction. J Comput Chem 2006;27:1787–99. https://doi.org/10.1002/jcc.20495.

[43] Monkhorst HJ, Pack JD. Special points for Brillouin-zone integrations. Phys Rev B 1976;13:5188–92. https://doi.org/10.1103/PhysRevB.13.5188.

[44] Zuluaga S, Liu LH, Shafiq N, Rupich SM, Veyan JF, Chabal YJ, et al. Structural band-gap tuning in g-C 3 N 4. Phys Chem Chem Phys 2015. https://doi.org/10.1039/c4cp05164e.

[45] Kanmani M, Lavanya R, Silambarasan D, Iyakutti K, Vasu V, Kawazoe Y. First principles studies on hydrogen storage in single-walled carbon nanotube functionalized with TiO_2. Sol. Stat. Comm. 2014;183:1–7. https://doi.org/10.1016/j.ssc.2013.12.017.